https://doi.org/10.3311/PPme.40894

Periodica Polytechnica Mechanical Engineering, 69(4), pp. 309–317, 2025

On the Tensile Behavior of Heat-treated Hydrogen Charged 316L Stainless Steel

Mariano N. Inés[1*], Graciela A. Mansilla[1]

[1] Laboratorio Metalurgia Física, Departamento Metalurgia, Facultad Regional San Nicolás, Universidad Tecnológica Nacional, Colón 332, 2900 San Nicolás de los Arroyos, Buenos Aires, Argentina
[*] Corresponding author, e-mail: mines@frsn.utn.edu.ar

Received: 05 May 2025, Accepted: 04 November 2025, Published online: 18 November 2025

Abstract

It is well established in the literature that the precipitation of different carbide types and intermetallic phases in stainless steels can lead to drastic consequences in their mechanical and corrosion behavior. Chromium carbide particles precipitate at grain boundaries, creating chromium depletion zones that expose the stainless steel to high corrosion penetration in harmful working atmospheres. The aim of this work is to evaluate the effect of electrolytically charged hydrogen on the mechanical behavior of heat treated AISI 316L austenitic stainless steel samples. To achieve a homogeneous distribution of carbides, specific heat treatments were conducted before tensile tests. Subsequently, a group of heat-treated samples were hydrogen-charged. After tensile tests carried out at high (0.003 s^{-1}) and low (0.000003 s^{-1}) strain rates, the resulting fracture surfaces exhibited mixed behavior in hydrogen-charged samples, i.e., ductile-brittle, in comparison with the ductile morphology obtained in uncharged ones. Additionally, in hydrogenated samples, cracks were associated with fine chromium carbides. Coincidentally, there was a ductility loss in hydrogen-charged samples, which was not observed in uncharged ones. In order to identify hydrogen-carbide interactions, combined studies of Differential Scanning Calorimetry (DSC) and a selective metallographic technique made it possible to identify grain boundaries and carbides/matrix interfaces as the main hydrogen traps. Finally, regarding strain rate effects on mechanical properties, it could be stated that when the strain rate decreases, the embrittlement effect of hydrogen is more explicitly manifested in conjunction with a microstructure sensitized by heat treatments and revealed by the mixed mode of fracture in hydrogen-charged samples.

Keywords

stainless steel, heat treatment, carbides, hydrogen embrittlement, DSC

1 Introduction

A considerable amount of attention is currently focused on austenitic stainless steels due to their superior corrosion resistance, surpassing that of martensitic and ferritic steels. These steels are characterized by excellent mechanical strength and oxidation resistance at high temperatures. They find wide applications in the oil industry and hydrogen energy services. Consequently, understanding hydrogen embrittlement (HE) mechanisms becomes crucial for establishing safe designs [1]. Given the intricate nature of HE phenomena, knowledge of hydrogen-structure interactions are essential to understand its entry into the alloy, transportation through the crystal lattice and interaction with crystal defects (such as vacancies, dislocations, grain boundaries, precipitates, inclusions, interfaces, etc.). The following two HE mechanisms are the most considered to explain the interaction of hydrogen with stainless steels:

1. Hydrogen-Enhanced Localized Plasticity (HELP) and
2. Hydrogen-Enhanced Decohesion (HEDE).

The HEDE mechanism postulates that the presence of hydrogen diminishes the cohesive strength of interface boundaries or lattice planes. Upon hydrogen ingress, the crystal lattice undergoes expansion, thereby compromising the strength of atomic bonds at the crack tip and consequently, the energy necessary for facilitating crack propagation is reduced, resulting in a macroscopic brittle fracture. Then, the HELP model is grounded in the hydrogen-enhanced dislocation mobility and dislocation slip behavior around a crack tip, leading to material softening [2, 3] and a decrease in Yield Strength (YS) [4, 5]. This softening eventually triggers [6] the premature initiation and growth of microvoids within local regions,

Cite this article as: Inés, M. N., Mansilla, G. A. "On the Tensile Behavior of Heat-treated Hydrogen Charged 316L Stainless Steel", Periodica Polytechnica Mechanical Engineering, 69(4), pp. 309–317, 2025. https://doi.org/10.3311/PPme.40894

resulting in reduced strength and ductility [7, 8] and highly localized fracture.

The novel HELP + HEDE model, proposed by [9–11], builds upon correlating mechanical properties with fractography analysis of fracture surfaces by means of scanning electron microscopy (SEM). This model establishes a link between the cooperative action of HELP and HEDE mechanisms in hydrogen embrittlement and the local concentration of hydrogen, providing a comprehensive experimental foundation beyond theoretical frameworks.

The accumulation of hydrogen at defects induces crack initiation and subsequent brittle fracture, thereby resulting in premature and catastrophic damage to engineering materials [12, 13]. Most importantly, understanding how hydrogen modifies the properties of the material is the key of those phenomena [2, 3, 9]. Despite the extensive literature on HE mechanisms, the local mechanisms of hydrogen interaction with austenitic stainless steels are not fully understood.

The presence of hydrogen in iron and steel alloys is typically an undesired occurrence because it adversely affects the physical and mechanical properties of metals and alloys. Hydrogen can be introduced through various means, including electrochemical processes, plating procedures, welding and exposure to hydrogen gas atmospheres. Studies have demonstrated that, during the electrolytic hydrogen charging of high-strength steels, the rate of hydrogen entry is influenced by factors such as the potential at the metal-electrolyte interface, the nature of the electrolytic solution, the presence of impurities in the electrolyte, and the charging time. These factors contribute to variations in the microhardness of steels [14]. Furthermore, as indicated by [15], certain elements considered as poisons can significantly impact the increase in hydrogen entry, even when present in relatively small concentrations. This phenomenon is observed during various operations such as acid pickling, corrosion, and cathodic charging.

The precipitation of various carbide types and intermetallic phases in stainless steels can be induced by heat treatments or continuous exposure to high-temperature operating environments. This phenomenon leads to significant alterations in the microstructure, consequently affecting the mechanical and corrosion properties of the material. For instance, the precipitation of carbides like $M_{23}C_6$, M_6C, and sigma phase can be detrimental in numerous applications. This is due to the creation of chromium depletion zones, exposing the steel to heightened corrosion penetration when used in adverse working atmospheres. Simultaneously, the reduced chromium concentration in adjacent areas sensitizes the steel to hydrogen capture during corrosive processes. This occurrence is most common in stainless steels with an austenitic and ferritic matrix, where carbides precipitate at various microstructural sites. Nevertheless, literature mentions that the hydrogen absorption capacity of AISI 316 steel is higher in the austenitic matrix than in different carbides and intermetallic phases. Brittle fractures associated with HE have been observed in stainless steels under severe environmental conditions, such as cathodic charging. Depending on test conditions and material sensitivity to HE, various fracture modes are observed in Fe–Ni–Cr alloys, including intergranular fracture, quasi-cleavage, twin boundary separation, and dimpled failure. In cases of brittle failures associated with HE, influence of hydrogen on the morphology of microvoids (with low spatial density) has been observed. However, this influence varies based on the material and hydrogen charging conditions.

On the other hand, when the material is subjected to mechanical stresses, the morphology and distribution of carbides can induce cracking effects, a phenomenon that may be further intensified by the presence of hydrogen. Some authors argue that networked carbides deteriorate certain properties of the steel, while fine and spherical carbides can serve as resistance sites against crack propagation, thereby improving mechanical properties. It is evident that carbide morphology can significantly influence the tensile behavior of steels [16].

Despite its widespread use, the mechanical response of 316 stainless steels has not been extensively characterized. The strain rate plays a pivotal role in describing the material response associated with hydrogen content in these types of stainless steels. For instance, authors in [17] conducted experiments on hydrogenated samples of duplex stainless steel at high (10^5 s^{-1}) and low (10^{-7} s^{-1}) tensile strain rates. They observed that quasi-static experiments showed an increment of approximately 20% in yield strength, which was linked to the deformation rate during the experiment. However, despite possessing favorable mechanical properties under low strain rate conditions, their responses under higher strain rates are consistently under consideration [18, 19].

Furthermore, as reported in [20], a correlation between strain rate and fracture surface characteristics was identified in a 304LN stainless steel. The analysis revealed that at lower strain rates, the void density was higher, and the average circular diameter of voids was lower, results that coincide with those expressed by [21]. This condition was associated

with higher strength and lower ductility. Conversely, at high strain rates, a reverse correlation between void features and mechanical properties was observed.

This article explores the tensile behavior of an AISI 316L austenitic stainless steel, heat treated and electrolytically hydrogen charged, tested under different strain rates.

2 Material and methods

Tensile samples were extracted from sheets of AISI 316L stainless steel. The chemical composition of the material is given in Table 1.

In order to evaluate carbides precipitation at grain boundaries, two different cooling conditions during heat treatment were applied, as summarized in Table 2. The objective was to achieve homogeneous distribution of carbides on these sites.

Prior to conducting tensile tests, a group of heat-treated samples were charged with hydrogen by means of the cathodic permeation method using graphite anode and constant current density of 35 mA/cm^2 for 3.5 h. An electrolytic solution of 1 N H_2SO_4 was employed with the addition of 0.25 g/L of $NaAsO_2$, which inhibits the recombination reaction of the H in aqueous solutions, thereby increasing the charge of atomic H into the sample. Once electrolytically charged, the specimens were carefully cleaned, dried and put into sealed recipients till the mechanical tests were carried out. Then all samples were tested under uniaxial tension in a 600 kN Universal Testing Machine (Model WDW-600S), at two different strain rates, that is, 3×10^{-3} s^{-1} and 3×10^{-6} s^{-1} (quasi-static tensile deformation). To ensure the repeatability and reproducibility of experimental results, the tests were conducted at least two times, and the average values are reported here.

Conventional metallographic characterization methods including location, distribution and shape of carbides were firstly performed by optical microscopy (Olympus GX51) while more detailed microstructure analysis of carbides and fracture surface after tensile test were conducted by scanning electron microscopy (SEM, LEITZ AMR 1000). Energy dispersive X-ray spectroscopy (EDS) was also employed. Furthermore, special silver reduction and decoration method presented by [22] was employed. This method consists of placing the sample into a chemical solution which contains silver ions. As a consequence of a redox reaction, the silver ions in contact with runaway H atoms reduce Ag ions into metallic Ag particles as expressed by the following reaction:

$$Ag^+ + H = Ag + H^+.$$

Those particles are precipitated on the surface of the sample thereby indicating sites where H was occluded. When metallographic samples are observed with SEM, those irregular Ag particles look bright and can be identified by EDS analysis.

Table 1 Chemical composition of AISI 316L austenitic stainless steel

Comp.	Fe	C	Si	Cr	Mn	Ni	Mo
Mass%	Bal	0.032	0.65	17.2	1.5	10.7	2.57

Table 2 Heat treatments parameters applied to specimens

Sample	Temperature [°C]	Time [min]	Cooling media
SSW	900	120	Water
SSA	900	120	Air

3 Results and discussion

3.1 Characterization of heat-treated samples

Microstructural characterization was conducted on AISI 316L austenitic stainless steel to analyze carbide sizes, distributions, and morphologies after annealing treatment at 900 °C for 120 minutes. A fully austenitic microstructure with isolated small globular chromium carbides was identified. The carbide mean size was 1–2 microns in water-cooled samples (SSW) and 1–4 microns in air-cooled ones (SSA), primarily located at austenitic grain boundaries. Globular geometry predominated, although irregular morphologies were also detected. EDS analysis confirmed a decrease in matrix chromium content near precipitate/matrix interfaces compared to the as-received sample (AR). This decrease could be attributed to a complex precipitation reaction, rendering susceptibility to embrittlement and intergranular corrosion when exposed to adverse working environments [23]. In AR samples, microscopy analysis revealed dense alignments of carbide particles, with a maximum length of 160 microns and an average diameter of 2.42 microns. After heat treatment with air cooling, the aligned carbide distribution became more widely spaced than in the AR samples. Moreover, for heat-treated samples, regardless of the cooling severity, a 3% increase in the amount of carbides was observed compared to the AR condition. The majority of these carbides were identified as $M_{23}C_6$ type, in accordance with thermodynamic simulations of thermal treatments performed using FactSage 8.0. Additionally, in air-cooled samples, a continuous gray phase was identified at austenitic grain boundaries, which could again be γCrC, FeC, MoC, NiC, CrN, NiN, and (Mn, Fe)S in accordance with the simulations above mentioned.

It is noteworthy that a greater quantity of carbides was formed with air cooling compared to those subjected to accelerate cooling in water. This observation was confirmed using image analysis software (Material Plus integrated into the Olympus GX51 microscope), revealing an increment of 1.5% in the number of carbides in SSA samples compared to SSW samples. This behavior could be attributed to the rapid cooling rates (water) that did not allow enough time for the proper growth (nucleation and development) of chromium carbides at austenitic grain boundaries. This, in turn, led to a smaller quantity of carbides developed at these sites. This finding aligns with [24], who, in its study on the effect of cooling rates on carbide precipitates and microstructure of 9Cr-1Mo oxide dispersion strengthened steel, noted that carbide precipitation becomes smaller and more widely dispersed as the cooling rate increases.

Additionally, differential scanning calorimetry (DSC) tests were performed to determine hydrogen desorption temperatures associated with specific trap sites in the austenitic stainless steel. The results revealed two distinct areas with hydrogen desorption peaks which corresponds to low-energy trapping zones for hydrogen: one around 200 °C (0.5 J/mol) and another between 450 °C and 590 °C (3 J/mol). The first zone possibly corresponds to traps of the reversible type, such as dislocations and vacancies, indicated by low-temperature desorption peaks [25]. The second area, with the higher energy value, could be linked to irreversible traps, specifically those associated with $M_{23}C_6$/matrix interfaces.

3.2 Effect of hydrogen on mechanical properties

As previously explained, air-cooled heat-treated sample SSA (from now on designated as TT samples) developed a larger quantity of carbides, leading to an increased number of hydrogen trapping sites. Consequently, their mechanical response was assessed, and potential interactions of hydrogen with the microstructure were identified. Fig. 1 presents the tensile test results for both as-received and heat-treated air-cooled austenitic stainless steel samples, with and without hydrogen charging, at strain rates of 3×10^{-3} s^{-1} and 3×10^{-6} s^{-1}.

In general terms, the highest values of Yield Strength (YS) and Ultimate Tensile Strength (UTS) are observed at higher strain rates, Fig. 1 (a), (b), as is typically expected for metallic materials.

On the other hand, the presence of hydrogen results in a slight decrease in the elongation to failure (i.e., TT – TT + H), depending on the strain rate, Fig. 1 (c).

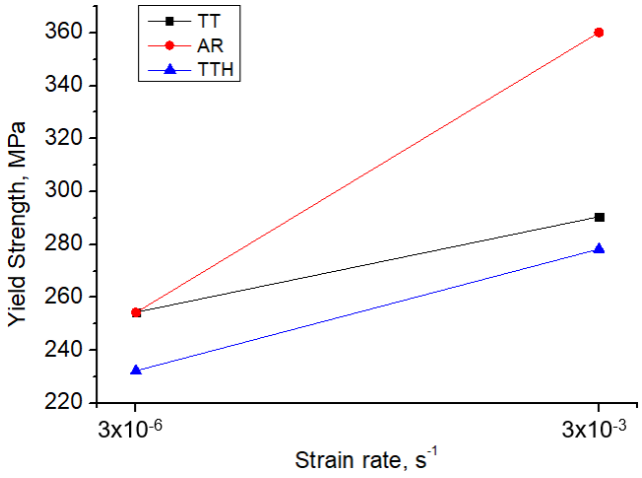

(a)

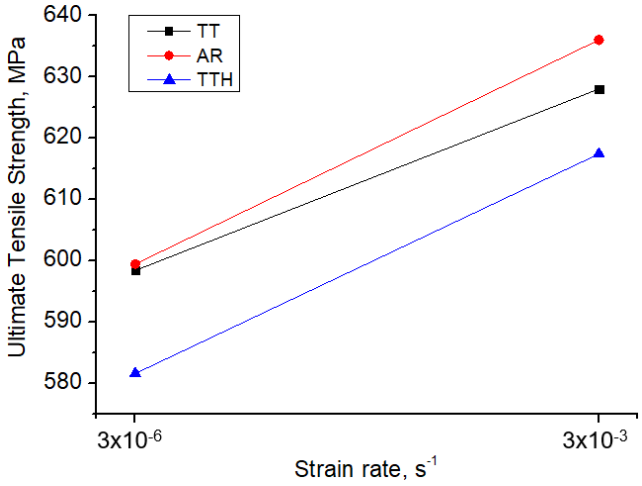

(b)

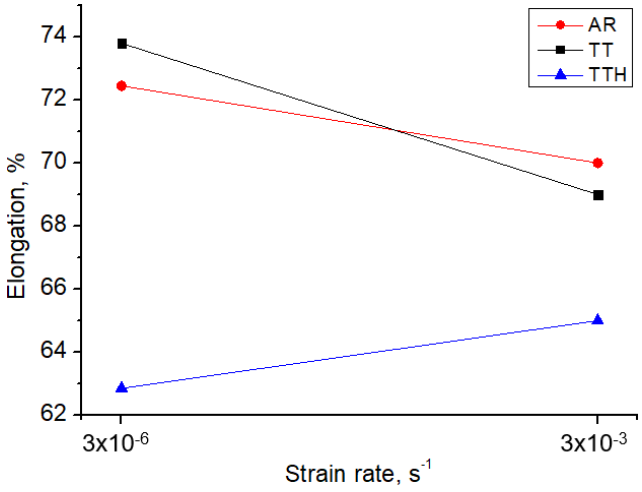

(c)

Fig. 1 Strain rate dependency with: (a) yield strength, (b) ultimate tensile strength and (c) elongation to failure of samples uncharged and H charged

However, when ductility or elongation to failure is analyzed concerning a specific strain rate, it becomes evident that samples with hydrogen exhibit lower values compared

to those without hydrogen. In other words, the presence of hydrogen renders the material more brittle, aligning with findings reported in the literature. The detrimental effect of hydrogen is particularly pronounced in the case of elongation, especially at strain rates around 3×10^{-6} s^{-1}.

Moreover, in Fig. 1 (a), there is a notable coincidence in YS point at the lower strain rate for both AR and TT samples. However, at higher strain rates, the difference between them increases to about 60 MPa. On the other hand, the presence of hydrogen further amplifies this difference (80 MPa) and is associated with the lower YS.

When considering strain rate effect on UTS, Fig. 1 (b), again H trapped assist deformation mechanisms causing constant stress difference for as received and heat treated - hydrogen charged samples (~20 MPa).

Now, when examining the impact of hydrogen on ductility loss for TT samples, Fig. 1 (c), the results indicate a more marked reduction in the sample tested at the lower strain rate (3×10^{-6} s^{-1}) compared to the sample tested at the higher ones (3×10^{-3} s^{-1}). To explicitly assess the extent of degradation, the [26] proposes the HE index, defined as Eq. (1) and calculated based on the difference in elongation to failure between samples with and without hydrogen charging.

$$I(\delta)\% = \left[\left(\left(\delta_{\text{uncharged}} - \delta_{\text{charged}}\right)/\delta_{\text{uncharged}}\right) \times 100\right] \quad (1)$$

Where $\delta_{\text{uncharged}}$ and δ_{charged} are the elongations to failure of heat-treated uncharged and hydrogen-charged samples, respectively. The index $I(\delta)$ values are plotted in Fig. 2. As observed from the results, the HE index is relatively small at a strain rate around 3×10^{-3} s^{-1}, and it increases with decreasing strain rate (3×10^{-6} s^{-1}). This behavior underscores the significance of hydrogen transport with dislocations during plastic deformation [27].

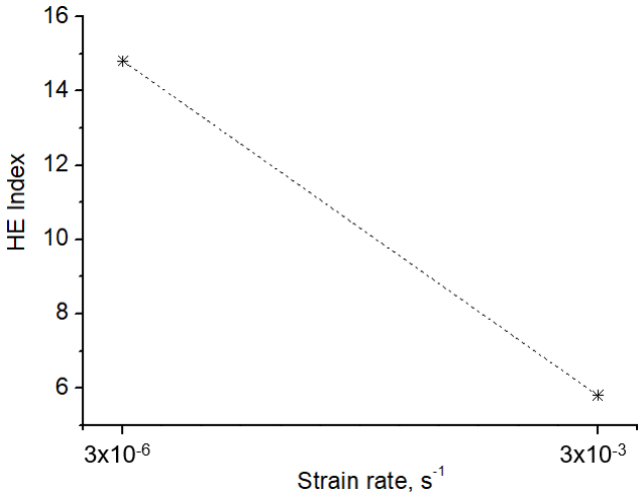

Fig. 2 Strain rate dependency with HE index

As a summary, the results demonstrated a reduction in tensile strength, yield strength and ductility of AISI 316L as a consequence of hydrogen charging, findings that align with those determined by [25]. These results can be correlated with the fact that HE is based on the diffusion of hydrogen, as mentioned by the authors in the context of hydrogen-charged duplex stainless steel [17, 26].

Additionally, hydrogen is likely released during the tensile test, and only when hydrogen has enough time for diffusion, as seen in the case of lower strain rate experiments, does its real effect on the behavior of AISI 316L with hydrogen charging become evident.

This argumentation is in line with that presented by [28], who asserted that strain rate influences the density and velocity of mobile dislocations. The interaction between hydrogen and dislocation depends on strain rate. Hydrogen can be transported by mobile dislocation easily under small strain rate due to the low dislocation mobility. The increase of hydrogen transport results in increasing dislocation activity in some local sites because of hydrogen-enhanced plasticity. At the same time, the increased dislocation activity enhances the hydrogen transport effects [29]. Therefore, the strain rate influences the interaction between hydrogen and dislocations, consistent with situations plotted in Fig. 1.

According to Fig. 1 (c) and focusing on the lower strain rate (3×10^{-6} s^{-1}), there is an almost 15% reduction in elongation at fracture when comparing the sample with heat treatment and hydrogen charging to its counterpart subjected only to heat treatment, and a 13% reduction when compared to the as-received sample.

The fracture surfaces in Fig. 3 in the hydrogenated sample exhibited external edges with indications of ductile fracture behavior (Fig. 3 (e), (f)), characterized by the coalescence of microvoids and the presence of Ni-Cr carbide particles inside them, as determined by EDS analysis. However, in the central regions of the sample (Fig. 3 (g), (h)), a large number of cracks and fracture plates associated with brittleness were evident. The ductile region is characterized by oriented and elongated dimples, suggesting a fracture enhanced by hydrogen, as indicated by [30].

As received and heat treated samples presented only dimples (plastic deformation). This ductile behavior determined in these samples and in hydrogenated ones (Fig. 3 (e), (f)), considering both strain rates, is likely caused by the coalescence of microvoids associated with carbides, potentially acting as initiation sites for cracks. As highlighted in [31], the quasi-cleavage surfaces observed in central regions of hydrogen-charged samples could result

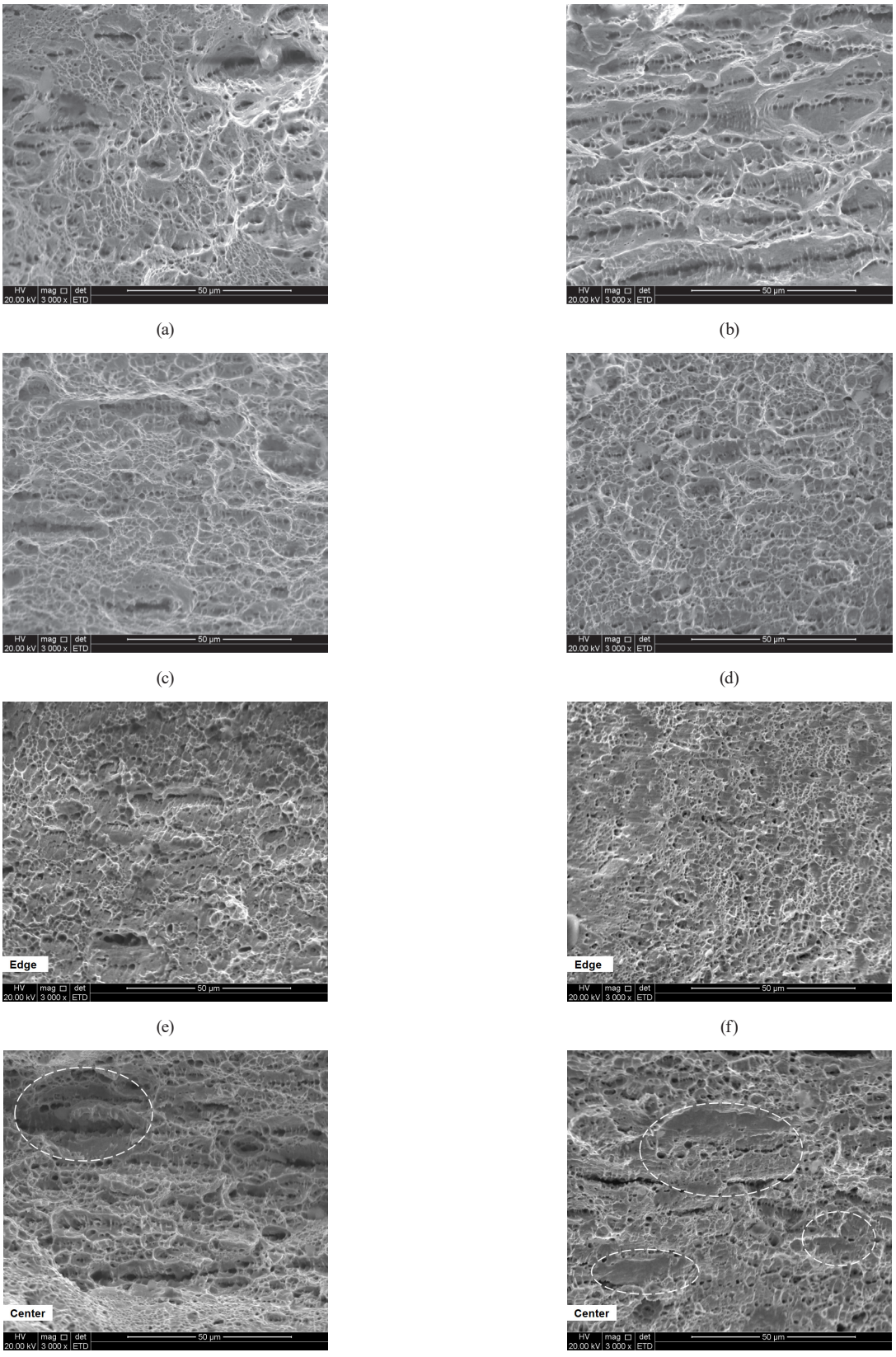

(a) (b)

(c) (d)

(e) (f)

(g) (h)

Fig. 3 SEM images of tensile fracture surfaces of AISI 316L stainless steel: (a) AR condition, strain rate 3×10^{-3} s^{-1}, (b) AR condition, strain rate 3×10^{-6} s^{-1}, (c) heat-treated air-cooled sample, strain rate 3×10^{-3} s^{-1}, (d) heat-treated and air-cooled sample, strain rate 3×10^{-6} s^{-1}, (e) heat-treated and air-cooled with H charging sample, strain rate 3×10^{-3} s^{-1}, (f) heat-treated and air-cooled with H charging sample, strain rate 3×10^{-6} s^{-1}, (g) heat-treated and air-cooled with H charging sample, strain rate 3×10^{-3} s^{-1}, (h) heat-treated and air-cooled with H charging sample, strain rate 3×10^{-6} s^{-1}

from the propagation of a ductile crack. The development of this ductile crack, arising from the coalescence of microvoids, could give rise to brittle, controlled facets influenced by hydrogen accumulation, as depicted in Fig. 3 (h). This intensification and localization of plastic deformation in the steel denotes the embrittlement behavior of samples with hydrogen in comparison to those of the as-received type, and it is maximized at the lowest strain rate tested in this study. Brittle fracture surfaces, as shown in Fig. 3 (g), (h), are evident by the presence of more faceted dimples, which lead to brittle fractures characterized by the formation of plates.

However, when samples without and with H charging are considered, there is a noticeable transition from a network of big dimples to smaller ones, Fig. 4, determined using quantitative calculations carried out with digital analysis software (scanning electron microscope (SEM)). Moreover, the fracture surface of hydrogenated samples consists of smaller, shallower voids, which in turn are orientated to the strain direction, as depicted in Fig. 3.

Furthermore, when considering the lower strain rate, the density of big dimples decreases, evolving into finer structures compared to those obtained at the higher strain rate (3×10^{-3} s^{-1}). This dimples observation seems to correspond well with the reduced UTS observed in samples tested at the lower strain rate (3×10^{-6} s^{-1}).

In summary, the largest reduction in elongation at fracture of hydrogen-charged samples tested were determined at a strain rate of 3×10^{-6} s^{-1} and could be attributed to the synergistic involvement of two HE micromechanisms: HELP and HEDE. As previously mentioned, HELP model is grounded in the hydrogen-enhanced dislocation mobility, leading to material softening and a decrease in YS, as was confirmed in this research. This softening generates the nucleation and growth of microvoids within local regions, resulting in reduced strength and ductility [7, 8] and highly localized fracture. As can be seen from Fig. 3, part of the fracture surface of the hydrogenated samples (Fig. 3 (g), (h)) presented smaller and shallower dimples compared to those without electrolytic H charging (Fig. 3 (c), (d)) at the same area (sample boundary), all of this was corroborated in Fig. 4. This is evidence that supports the lower values of mechanical resistance found in the samples with H, in agreement with the observations made by [32] for an austenitic stainless steel 316H cathodically charged with hydrogen.

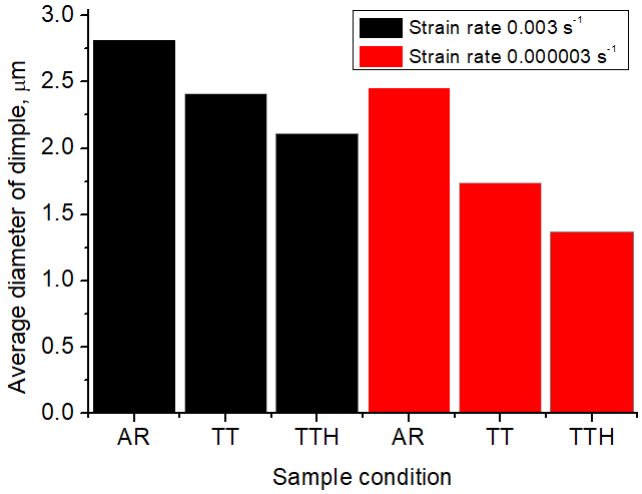

Fig. 4 Variation of average diameter of dimples with strain rate

On the other hand, the HEDE mechanism provides greater understanding of the mixed fracture mode, that is, ductile-brittle, found in the sample with electrolytic hydrogen charge (Fig. 3 (h)), with clear evidence of brittle plates that were determined by SEM microscopy observations.

These preliminary findings align with SEM observations, where carbide particles and grain boundaries were identified as trap sites for hydrogen, employing Ag microprint technique and SEM observation with dispersive energy analysis-EDS as illustrated in Fig. 5.

Generally, and in concurrence with [33], as the strain rate decreases, the embrittlement effect of hydrogen becomes more pronounced, particularly in tandem with a microstructure sensitized by heat treatments, as evidenced by the mixed mode of fracture observed in hydrogen-charged samples [34], the larger reduction in ductility (increase in brittleness) and the higher value of the HE indexes. Finally, the cracks identified in the hydrogenated material likely resulted from the combined effect of microvoid coalescence and hydrogen trapping.

4 Conclusion

The data on strain rate and mechanical properties indicate that hydrogen charging influences the dynamics of dislocations and fracture micromechanisms in AISI 316L heat treated and hydrogen-charged samples. The coupled effect of precipitates developed during heat treatment and hydrogen, assists softening, leading to a decrease in yield strength.

Based on the results determined in this work, it can be stated that when the strain rate decreases, the hydrogen embrittlement effect is more explicitly manifested. Dislocation transport of hydrogen assists in this way Hydrogen-Enhanced Localized Plasticity (HELP), as dominating deformation mechanism and causing specimen fracture via transgranular cracking, at the same time

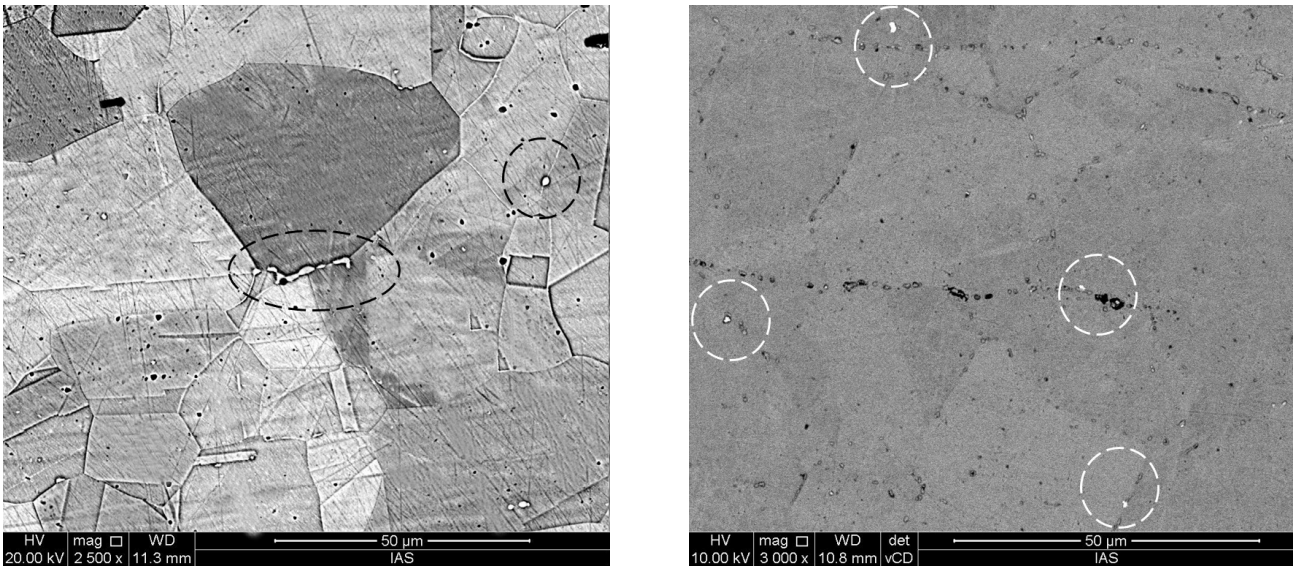

(a) (b)

Fig. 5 SEM images showing Ag particles (white) associated with hydrogen at: (a) grain boundaries, and (b) carbide particles

Hydrogen-Enhanced Decohesion (HEDE) mechanism becomes most important, and responsible of mixed fracture surfaces associated with H charged samples.

References

[1] Hatano, M., Fujinami, M., Arai, K., Fujii, H., Nagumo, M. "Hydrogen embrittlement of austenitic stainless steels revealed by deformation microstructures and strain-induced creation of vacancies", Acta Materialia, 67, pp. 342–353, 2014. https://doi.org/10.1016/j.actamat.2013.12.039

[2] Barrera, O., Bombac, D., Chen, Y., Daff, T. D., Galindo-Nava, E., Gong, P., Haley, D., Horton, R., Katzarov, I., Kermode, J. R., Liverani, C., Stopher, M., Sweeney, F. "Understanding and mitigating hydrogen embrittlement of steels: a review of experimental, modelling and design progress from atomistic to continuum", Journal of Material Science, 53(9), pp. 6251–6290, 2018. https://doi.org/10.1007/s10853-017-1978-5

[3] Djukic, M. B., Zeravcic, V. S., Bakic, G., Sedmak, A., Rajicic, B. "Hydrogen embrittlement of low carbon structural steel", Procedia Materials Science, 3, pp. 1167–1172, 2014. https://doi.org/10.1016/j.mspro.2014.06.190

[4] Lukito, H., Szklarska-Smialowska, Z. "Susceptibility of medium-strength steels to hydrogen-induced cracking", Corrosion Science, 39(12), pp. 2151–2169, 1997. https://doi.org/10.1016/S0010-938X(97)00099-1

[5] Araújo, B. A., Travassos, G. D., Silva, A. A., Vilar, E. O., Carrasco, J. P., De Araújo, C. J. "Experimental characterization of hydrogen embrittlement in API 5L X60 and API 5L X80 steels", Key Engineering Materials, 478, pp. 34–39, 2011. https://doi.org/10.4028/www.scientific.net/KEM.478.34

[6] Kim, Y., Kim, Y., Kim, D., Kim, S., Nam, W., Choe, H. "Effects of hydrogen diffusion on the mechanical properties of austenite 316L steel at ambient temperature", Materials Transactions, 52(3), pp. 507–513, 2011. https://doi.org/10.2320/matertrans.M2010273

[7] Wu, X. Q., Kim, I. S. "Effects of strain rate and temperature on tensile behavior of hydrogen-charged SA508 Cl.3 pressure vessel steel", Materials Science and Engineering: A, 348(1–2), pp. 309–318, 2003. https://doi.org/10.1016/S0921-5093(02)00737-2

[8] Kim, I. S. Kang, S. S. "Dynamic strain aging in SA508-class 3 pressure vessel steel", International Journal of Pressure Vessels and Piping, 62(2), pp. 123–129, 1995. https://doi.org/10.1016/0308-0161(95)93969-C

[9] Djukic, M. B., Bakic, G. M., Sijacki Zeravcic, V., Sedmak, A., Rajicic, B. "The synergistic action and interplay of hydrogen embrittlement mechanisms in steels and iron: Localized plasticity and decohesion", Engineering Fracture Mechanics, 216, 106528, 2019. https://doi.org/10.1016/j.engfracmech.2019.106528

[10] Djukic, M. B., Sijacki Zeravcic, V., Bakic, G. M., Sedmak, A., Rajicic, B. "Hydrogen damage of steels: A case study and hydrogen embrittlement model", Engineering Failure Analysis, 58, pp. 485–498, 2015. https://doi.org/10.1016/j.engfailanal.2015.05.017

[11] Djukic, M. B., Bakic, G. M., Zeravcic, V. S., Sedmak, A., Rajicic, B. "Hydrogen embrittlement of industrial components: prediction, prevention, and models", Corrosion, 72(7), pp. 943–961, 2016. https://doi.org/10.5006/1958

[12] Song, J., Curtin, W. A. "Atomic mechanism and prediction of hydrogen embrittlement in iron", Nature Materials, 12(2), pp. 145–151, 2013. https://doi.org/10.1038/nmat3479

[13] Momida, H., Asari, Y., Nakamura, Y., Tateyama, Y., Ohno, T. "Hydrogen-enhanced vacancy embrittlement of grain boundaries in iron", Physical Review B, 88(14), 144107, 2013. https://doi.org/10.1103/PhysRevB.88.144107

[14] Candia, G. L., Brandaleze, E., Mansilla, G. A. "Estudio del efecto del hidrógeno sobre la midrodureza de acero" (Study of the hydrogen effect on microhardness of steels), Revista de Ciencia y Tecnología, 15(19), pp. 64–68, 2013. (in Spanish)

[15] Patty, B. B., Das, C. R., Singh, D. D. N. "Role of hydrogen promoters on corrosion and hydrogenation of mild steel in aqueous and methanolic hydrochloric acid solutions", Corrosion, 51(7), pp. 537–543, 1995.
https://doi.org/10.5006/1.3294374

[16] Yu, E., Jung, H., Kim, K.-S., Kim, E.-J., Kim, J. "Influence of carbide formation on tensile and fatigue properties of carburized steels", Applied Microscopy, 43(2), pp. 81–87, 2013.
https://doi.org/10.9729/am.2013.43.2.81

[17] Silverstein, R., Eliezer, D. "Hydrogen trapping energy levels and hydrogen diffusion at high and low strain rates (10^5 s^{-1} and 10^{-7} s^{-1}) in lean duplex stainless steel", Materials Science and Engineering: A, 674, pp. 419–427, 2016.
https://doi.org/10.1016/j.msea.2016.08.019

[18] Acharya, S., Moitra, A. Bysakh, S., Nanibabu, M. Krishanan, S. A., Mukhopadhyay, C. K., Rajkumar, K. V., Sasikala, G., Mukhopadhyay, A., Mondal, D. K., Ghosh, K. S., Jha, B. B., Muraleedharan, K. "Effect of high strain rate deformation on the properties of SS304L and SS316LN alloys", Mechanics of Materials, 136, 103073, 2019.
https://doi.org/10.1016/j.mechmat.2019.103073

[19] Jin, H., Sanborn, B., Lu, W.-Y., Song, B. "Mechanical characterization of 304L-VAR stainless steel in tension with a full coverage of low, intermediate, and high strain rates", Mechanics of Materials, 152, 103654, 2021.
https://doi.org/10.1016/j.mechmat.2020.103654

[20] Das, A., Sivaprasad, S., Chakraborti, P. C., Tarafder. S. "Correspondence of fracture surface features with mechanical properties in 304LN stainless steel", Materials Science and Engineering: A, 496(1–2), pp. 98–105, 2008.
https://doi.org/10.1016/j.msea.2008.05.007

[21] Das, A., Tarafder, S. "Geometry of dimples and its correlation with mechanical properties in austenitic stainless steel", Scripta Materialia, 59(9), pp. 1014–1017, 2008.
https://doi.org/10.1016/j.scriptamat.2008.07.012

[22] Schober, T., Dieker, C. "Observation of local hydrogen on nickel surfaces", Metallurgical Transactions A, 14(11), pp. 2440–2442, 1983.
https://doi.org/10.1007/BF02663321

[23] Rozenak, P., Eliezer, D. "Precipitation behaviour of sensitized AISI type 316 austenitic stainless steel in hydrogen", Journal of Materials Science, 21(9), pp. 3065–3070, 1986.
https://doi.org/10.1007/BF00553337

[24] Jang, K.-N., Kim, T.-K., Kim, K.-T. "The effect of cooling rates on carbide precipitate and microstructure of 9CR-1MO oxide dispersion strengthened (ODS) steel", Nuclear Engineering and Technology, 51(1), pp. 249–256, 2019.
https://doi.org/10.1016/j.net.2018.09.021

[25] Ye, F., Zhu, T., Mori, K., Xu, Q., Song, Y., Wang, Q., Yu, R., Wang, B., Cao, X. "Effects of dislocations and hydrogen concentration on hydrogen embrittlement of austenitic 316 stainless steels", Journal of Alloys and Compounds, 876, 160134, 2021.
https://doi.org/10.1016/j.jallcom.2021.160134

[26] Yousefi, A., Itoh, G. "Tensile properties of an electrolytically hydrogen charged duplex stainless steel affected by strain rate", ISIJ International, 58(3), pp. 561–565, 2018.
https://doi.org/10.2355/isijinternational.ISIJINT-2017-631

[27] Astafurova, E., Fortuna, A., Melnikov, E., Astafurov, S. "The effect of strain rate on hydrogen-assisted deformation behavior and microstructure in AISI 316L austenitic stainless steel", Materials, 16(8), 2983, 2023.
https://doi.org/10.3390/ma16082983

[28] Hong, Y., Zhou, C., Zheng, Y., Zhang, L., Zheng, J., Chen, X. "Effect of hydrogen and strain rate on nanoindentation creep of austenitic stainless steel", International Journal of Hydrogen Energy, 44(2), pp. 1253–1262, 2019.
https://doi.org/10.1016/j.ijhydene.2018.11.017

[29] Dadfarnia, M., Martin, M. L., Nagao, A., Sofronis, P., Robertson, I. M. "Modeling hydrogen transport by dislocations", Journal of the Mechanics and Physics of Solids, 78, pp. 511–525, 2015.
https://doi.org/10.1016/j.jmps.2015.03.002

[30] San Marchi, C., Somerday, B. P., Tang, X., Schiroky, G. H. "Effects of alloy composition and strain hardening on tensile fracture of hydrogen-precharged type 316 stainless steels", International Journal of Hydrogen Energy, 33(2), pp. 889–904, 2008.
https://doi.org/10.1016/j.ijhydene.2007.10.046

[31] Merson, E. D., Poluyanov, V. A., Merson, D. L., Vinogradov, A. Y. "About the nature of quasi-cleavage in low-carbon steel embrittled with hydrogen", Metal Science and Heat Treatment, 61(3), pp. 191–195, 2019.
https://doi.org/10.1007/s11041-019-00399-x

[32] Falat, L., Čiripová, L., Petryshynets, I., Milkovič, O., Džupon, M., Kovaľ, K. "Hydrogen embrittlement behavior of plastically prestrained and cathodically hydrogen-charged 316H grade austenitic stainless steel", Crystals, 12(10), 1419, 2022.
https://doi.org/10.3390/cryst12101419

[33] Díaz, G. Á., Suárez, T. E. G., González, C. R., Varela F. J. B. "Effect of the strain rate on the fracture behaviour of high pressure pre-charged samples", Proceedings, 2(23), 1417, 2018.
https://doi.org/10.3390/proceedings2231417

[34] Inés, M. N., Mansilla, G. A. "Efecto de la velocidad de deformación en ensayos de tracción de acero inoxidable AISI 316L" (Effect of strain rate on tensile tests of AISI 316L stainless steel), Ajea (Actas de Jornadas y Eventos Académicos de UTN), 12, pp. 1241–1251, 2021. (in Spanish)
https://doi.org/10.33414/ajea.7.867.2021